The Source-Stabilized Galerkin Formulation for Linear Moving Conductor Problems With Edge Elements

Sujata Bhowmick[1] and Sethupathy Subramanian[2]

[1]Department of Electronics System Engineering, Indian Institute of Science, Bangalore 560012, India
[2]Department of Physics and Astronomy, University of Notre Dame, Notre Dame, IN 46556 USA

The phenomenon of linear motion of conductor in a magnetic field is commonly found in electric machineries, such as electromagnetic brakes, linear induction motor, electromagnetic flowmeter, and so on. The design and analysis of the same require an accurate evaluation of induced currents and the associated reaction magnetic fields. The finite-element method (FEM) is a generally employed numerical technique for this purpose. However, it needs stabilization techniques to provide an accurate solution. In this work, such a stabilization technique is developed for the edge elements. The stability and, hence, the accuracy are brought in by a suitable representation of the source term. The stability and accuracy of the proposed scheme are first shown analytically and then demonstrated with the help of 2-D and 3-D simulations. The proposed scheme would require a graded regular mesh along the direction of motion.

Index Terms— **Edge element, magnetic advection, moving conductor, numerical stability, Z transform.**

I. Introduction

THE numerical simulation of electrical machineries and equipment is inevitable for their economical design and safe operation. The finite-element method (FEM) is a commonly employed numerical technique. The FEM is known to produce highly accurate solutions for second-order diffusive simulations. The same is not true when dominant first-order terms are present. The governing equations of conductor moving in a magnetic field fall into this category. Consider the following governing equations of conductor moving in a magnetic field $\mathbf{B_a}$ [1], [2]:

$$\sigma\nabla\phi - \left(\nabla\cdot\frac{1}{\mu}\nabla\right)\mathbf{A} - \sigma\mathbf{u}\times\nabla\times\mathbf{A} = \sigma\mathbf{u}\times\mathbf{B_a} \quad (1)$$

$$\nabla\cdot(\sigma\nabla\phi) - \nabla\cdot(\sigma\mathbf{u}\times\nabla\times\mathbf{A}) = \nabla\cdot(\sigma\mathbf{u}\times\mathbf{B_a}) \quad (2)$$

where ϕ is the scalar potential arising out of the current flow, $\mathbf{A}$ is the magnetic vector potential associated with reaction magnetic field $\mathbf{b}$, $\mathbf{u}$ is the velocity of the moving conductor, μ is the magnetic permeability, and σ is electrical conductivity.

It can be seen that, for the variables $\mathbf{A}$ and ϕ, all the derivatives in (2) are second derivatives. So, this equation is not expected to introduce any instability in the solution. However, the same is not true for (1); here, the first derivative is present in the form of $\sigma\mathbf{u}\times\nabla\times\mathbf{A}$. When this becomes dominant, more precisely, when the quantity $\mu\sigma|\mathbf{u}|\Delta z/2$ becomes larger than 1, the numerical instability ensues, where Δz is the element length along the flow direction [3], [4], [5]. This quantity is called as Peclet number ($Pe = \mu\sigma|\mathbf{u}|\Delta z/2$).

In such a situation, to bring in stability and accuracy to numerical solutions, several numerical remedies have been proposed. Among these, the upwinding techniques are commonly used across disciplines. The upwinding schemes are proposed for the fluid dynamics transport equation and extended for the moving conductor problems [6], [7], [8], [9], [10], [11], [12], [13], [14], [15], [16]. The upwinding-based schemes can be inferred as to bring in the stability by introducing the right amount of diffusion [17], [18]. The *correct* amount of diffusion is decided by the stabilization parameter τ, which is defined to be $\tau = \coth(Pe) - 1/Pe$. On the other hand, the recent source-stabilized finite-element schemes are primarily proposed for the linear moving conductor problems [19], [20]. They do not seek stability by adding diffusion (upwinding) to the governing equation. Instead, stability is brought in by the appropriate representation of the source term, which mitigates numerical instability via pole-zero cancellation. In addition, the source-stabilizing schemes are shown to be free of non-physical currents at the material boundary [21].

It can be noted that, all of the above mentioned stabilization techniques are derived for the linear nodal elements for the 1-D problem of equal discretization, and they are heuristically extended for the 2-D and 3-D problems [17]. The one exception can be the source-stabilized scheme proposed in [20], where stability is analytically shown for a simplified 2-D problem.

In electrical engineering, edge elements are widely used to accommodate for the discontinuity of the normal field at the material interfaces; this is not possible with the nodal elements. It can be noted that, numerical instability at high velocities is present in the edge-element formulation as well. In order to cater this, there are upwinding techniques proposed for the moving conductor problems with the edge elements [22], [23]. These are generally based on the heuristic extension of the upwinding techniques proposed for the fluid dynamics transport equation. Hence, they are also susceptible to transverse-boundary error at the material interfaces [24], [25], [26], [27].

Manuscript received 30 May 2022; revised 8 January 2023 and 19 April 2023; accepted 11 July 2023. Date of publication 14 July 2023; date of current version 25 August 2023. Corresponding author: S. Bhowmick (e-mail: sujatabhowmick@gmail.com).

Color versions of one or more figures in this article are available at https://doi.org/10.1109/TMAG.2023.3295590.

Digital Object Identifier 10.1109/TMAG.2023.3295590

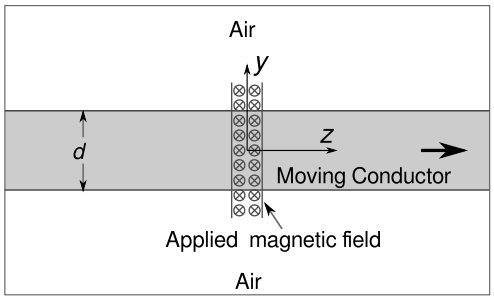

Fig. 1. Schematic of the 2-D problem.

In this work, an attempt is made to propose a source-stabilized Galerkin finite-element formulation for the edge elements. For this, a simplified version of the moving conductor problem is considered; using that, the stability of the proposed formulation is established. Then, in order to correctly represent the edge elements as well as the curl nature of the governing equation, an extensive stability analysis is carried out in 2-D. Subsequently, numerical exercises are carried out both in 2-D as well as 3-D.

In Section II, description of this work is provided, and it starts with the stability analysis for a simplified problem.

II. Present Work

A. Analysis With Limiting 1-D Version of the Problem

Stability analysis of a complete moving conductor problem is very difficult to handle, mainly due to the presence of multiple materials and the structure of the simulation domain. Therefore, a simplified moving conductor problem will be considered here, following a previous work [19]. A slightly modified version of the 2-D moving conductor problem used in [19] is shown in Fig. 1. In this, a conducting slab of thickness d is moving along the z-axis with velocity u_z, under the influence of magnetic field B_x directed along the x-axis. The conductivity and permittivity for the conductor are denoted as σ and μ, respectively.

For this 2-D problem, the vector potential has components of A_y and A_z. The same has been depicted in Fig. 2(a). In Fig. 2(a), the finite-element discretization of the 2-D problem using edge elements is shown for one y edge ($[n, m+1/2]$). For the sake of mathematical analysis, a simplified version with equal discretization along the z- and y-axes is chosen. The edge variables are subscripted with n and m, where n denotes the progression along the z-axis and m denotes the progression along the y-axis. It can be noted that, in addition to the integer progression ($n-1$, n, and $n+1$), a factor of $1/2$ is present to denote the edge variable that is constant for the edge.

Now, let us consider the limiting case of $d \to \infty$ as described in [19]. Here, due to the symmetry along the y-axis, the variations with respect to the y-axis vanish, resulting in a problem, which is independent of ϕ and A_z. This situation is depicted in Fig. 2(b), wherein only A_y has variations along the z-axis as is the case for y-directed edges, which have the natural variation along the z-axis (perpendicular axis).

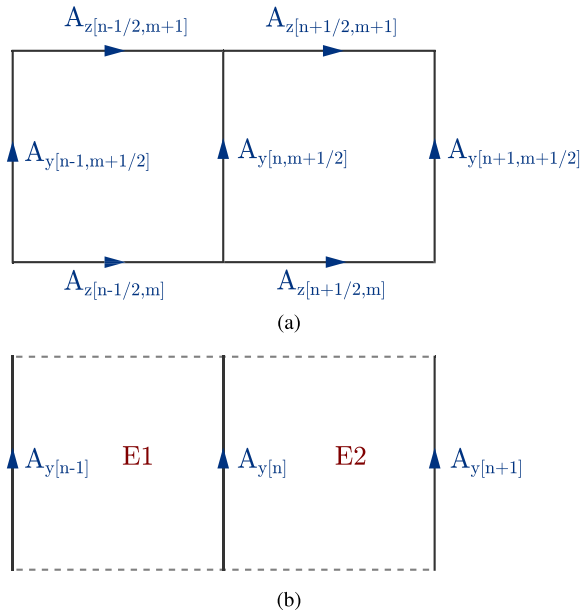

Fig. 2. Representation of $\mathbf{A}$ with edge elements in the zy plane. (a) 2-D. (b) Reduced 1-D.

The corresponding finite-element formulation using the edge elements can be written as follows:

$$\int_\Omega \frac{dM_y^l}{dz}\frac{dA_y}{dz}d\Omega + \mu\sigma u_z \int_\Omega M_y^l \frac{dA_y}{dz}d\Omega + \cdots = \mu\sigma u_z \int_\Omega M_y^l B_x \quad (3)$$

where M_y^l is the y-directed edge weight function [28]. Evaluating the above equation for the nth edge gives the following difference equation:

$$-(1+Pe)A_{y[n-1]} + 2A_{y[n]} - (1-Pe)A_{y[n+1]} + \cdots = \frac{1}{3}\left(B_{x[n-1]} + 4B_{x[n]} + B_{x[n+1]}\right)Pe\Delta z. \quad (4)$$

This is the same as that of the nodal formulation as in [20]. The numerical instability due to the negative roots (*poles*) of the difference equation can also be viewed with the help of Z transform [19], [20]. Moreover, the Z transform clearly shows the effect of *zeros* arising from the source term as well. Applying the Z transform on (4)

$$\frac{A_y}{B_x} = \frac{(Z+0.27)(Z+3.73)Pe\Delta z}{3(-1+Pe)(Z-1)\left(Z-\frac{-1-Pe}{-1+Pe}\right)}. \quad (5)$$

For $Pe \gg 1$, (5) reduces to

$$\frac{A_y}{B_x} \simeq \frac{\Delta z}{3}\frac{(Z+0.27)(Z+3.73)}{(Z-1)(Z+1)}. \quad (6)$$

Now, the pole at -1 of (6) leads to the oscillation in the solution.

Here, the relation between A_y and B_x in (6) is found to be same as that of in [20] with the nodal formulation. The oscillation appearing in the solution in [20] is successfully mitigated by applying the input field B_x as the averaged nodal flux densities for the element. Here, the same approach is extended for the edge formulation, with elemental input fields,

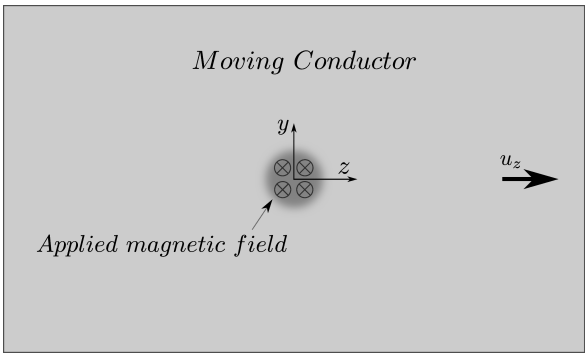

Fig. 3. Schematic of the simplified 2-D problem for the stability analysis.

B_{xE1} and B_{xE2}. The B_{xE1} and B_{xE2} are the element-averaged input magnetic fields for the elements spanning $[n-1]$, $[n]$ and $[n]$, $[n+1]$, respectively. The B_{xE1} and B_{xE2} are defined as follows [20]:

$$B_{xE1} = \big(B_{x[n-1]} + B_{x[n]}\big)/2$$
$$B_{xE2} = \big(B_{x[n]} + B_{x[n+1]}\big)/2.$$

For these modified inputs, the difference equation for (3) becomes

$$-(1+Pe)A_{y[n-1]} + 2A_{y[n]} - (1-Pe)A_{y[n+1]} + \cdots = \frac{1}{2}\big(B_{x[n-1]} + 2B_{x[n]} + B_{x[n+1]}\big)Pe\Delta z. \quad (7)$$

Applying the Z transform

$$\frac{A_y}{B_x} = \frac{(Z+1)^2 Pe\Delta z}{2(-1+Pe)(Z-1)\big(Z-\frac{-1-Pe}{-1+Pe}\big)}. \quad (8)$$

For $Pe \gg 1$, (8) reduces to

$$\frac{A_y}{B_x} \simeq \frac{\Delta z}{2}\frac{(Z+1)}{(Z-1)}. \quad (9)$$

While comparing (9) with (6), one would readily recognize that for high Peclet number, the zero at -1 for the second case eventually cancels the oscillatory pole at -1, thus leading to a stable solution. This indicates that the elemental average of the input magnetic field can be used for the edge elements as well. However, further confirmation in 2-D would be helpful, since the edge elements are generally designed for curl problems. The stability analysis in 2-D is dealt in Section II-B.

B. Analysis With the 2-D Version of the Problem

A simplified, 2-D version of the moving conductor problem, as shown in Fig. 3, is considered. The governing equations for the same are given as follows:

$$\nabla\cdot(\sigma\nabla\phi) - \nabla\cdot(\sigma\mathbf{u}\times(\nabla\times\mathbf{A})) = \nabla\cdot\big(\sigma u_z B_x\hat{y}\big) \quad (10)$$

$$\sigma\nabla\phi - \nabla\cdot\frac{1}{\mu}(\nabla\mathbf{A}) - \sigma\mathbf{u}\times(\nabla\times\mathbf{A}) = \sigma u_z B_x\hat{y}. \quad (11)$$

In the edge-element formulation, the magnetic vector potential $\mathbf{A}$ is modeled with the edge vector shape functions $\mathbf{M}$ [28]. For this cartesian case, the y component of the vector potential would be modeled with y-directed edge shape functions, and similarly, the z component of the vector potential would be modeled with z-directed edge shape functions. The electric scalar potential ϕ is modeled with the nodal shape functions N. In the Galerkin finite-element formulation, the weight functions are the shape functions themselves, and to mark the difference, the weight functions are super-scripted with l.

The Galerkin finite-element formulation for (10) and (11) can be written as follows:

$$\int_\Omega \frac{dN^l}{dz}\frac{d\phi}{dz}d\Omega + \int_\Omega \frac{dN^l}{dy}\frac{d\phi}{dy}d\Omega + u_z\int_\Omega \frac{dN^l}{dy}\frac{dA_y}{dz}d\Omega + \cdots - u_z\int_\Omega \frac{dN^l}{dy}\frac{dA_z}{dy}d\Omega = u_z\int_\Omega \frac{dN^l}{dy}B_x \quad (12)$$

$$\mu\sigma\int_\Omega M_y^l\frac{d\phi}{dy}d\Omega + \int_\Omega \frac{dM_y^l}{dz}\frac{dA_y}{dz}d\Omega + \int_\Omega \frac{dM_y^l}{dy}\frac{dA_y}{dy}d\Omega + \cdots + \mu\sigma u_z\int_\Omega M_y^l\frac{dA_y}{dz}d\Omega - \mu\sigma u_z\int_\Omega M_y^l\frac{dA_z}{dy}d\Omega + \cdots = \mu\sigma u_z\int_\Omega M_y^l B_x \quad (13)$$

$$\mu\sigma\int_\Omega M_z^l\frac{d\phi}{dz}d\Omega + \int_\Omega \frac{dM_z^l}{dz}\frac{dA_z}{dz}d\Omega + \int_\Omega \frac{dM_z^l}{dy}\frac{dA_z}{dy}d\Omega = 0. \quad (14)$$

It can be noted that, (13) and (14) are the weighted residual formulation of (11); the former arises from the y-directed edge weight function $\mathbf{M}^l = M_y^l$, and the latter arises from the z-directed edge weight function $\mathbf{M}^l = M_z^l$. In addition to this, for the rest of the analysis, the element lengths along the y- and z-directions are assumed to be equal, i.e., $\Delta y = \Delta z$ [20].

The difference form of the finite-element equation (12) for node 4 [see Fig. 4(b)] can be written as follows:

$$\frac{1}{6}\big(2\big(\phi_{[0]}+\phi_{[1]}+\phi_{[2]}+\phi_{[3]}-8\phi_{[4]}+\phi_{[5]}+\phi_{[6]}+\cdots + \phi_{[7]}+\phi_{[8]}\big) + 3u_z\big(A_{[e2]}-A_{[e0]}-A_{[e4]}-A_{[e6]}+\cdots + A_{[e10]}-A_{[e8]}+A_{[e11]}-A_{[e7]}\big)\big)+\cdots = \frac{u_z\Delta y}{12}\big(B_{x[8]}+B_{x[6]}+4B_{x[7]}-B_{x[0]}+\cdots - 4B_{x[1]}-B_{x[2]}\big). \quad (15)$$

In the above equation, it may be noted that the scalar variable ϕ is at the nodes, whereas the vector potential $A_{[e]}$ is present at the edges. The stability analysis requires the variables to be at the nodes [20], [29], [30]. Therefore, it is necessary to represent the vector potential at the nodes. For this, the node equivalent of the vector potential is obtained by averaging the vector potential at the edges. Each node has two y-directed edges (vertical edges); by taking the average of the two, the $A_{y[node]}$ is obtained. Similarly, each node has two z-directed edges (horizontal edges); by taking the average of the two, the $A_{z[node]}$ is obtained. With these, the nodal form of (15) can be written as follows:

$$\frac{1}{6}\big(2\big(\phi_{[0]}+\phi_{[1]}+\phi_{[2]}+\phi_{[3]}-8\phi_{[4]}+\phi_{[5]}+\phi_{[6]}+\cdots + \phi_{[7]}+\phi_{[8]}\big) + \frac{3u_z}{2}\big(A_{y[0]}+A_{y[8]}-A_{y[2]}-A_{y[6]}\big)+\cdots + 3u_z\big(-A_{z[1]}+A_{z[7]}\big)\big)+\cdots$$

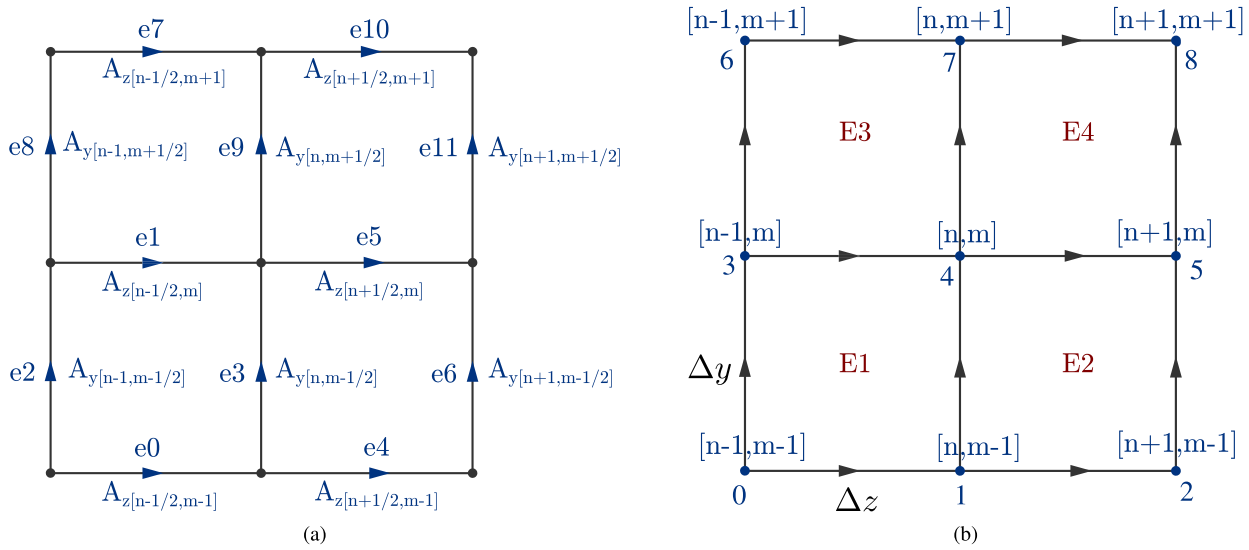

Fig. 4. Representation of edge elements in 2-D zy plane. (a) z- and y-directed edge vectors and their corresponding edge numbers. (b) Node and element numbering for the same set of edge elements.

$$= \frac{u_z \Delta y}{12}\big(B_{x[8]} + B_{x[6]} + 4B_{x[7]} - B_{x[0]} + \cdots - 4B_{x[1]} - B_{x[2]}\big). \quad (16)$$

For the vector equation, the 2-D representation [see Fig. 4(a)] has two edges for each direction. That is, the shape function corresponds to edges $e3$ and $e9$; each forms a finite-element equation. Similarly, the shape function corresponds to edges $e1$ and $e5$; each forms a finite-element equation. Thus, there are four finite-element equations associated with four edges. In contrast, the node element forms only one equation that corresponds to node 4. The edges $e1$ and $e5$ are directed along the z-direction, so their Galerkin weighted residual formulation corresponds to the z component of the vector equation (11). Then, the difference form of the finite-element equation (14) for $e1$ can be written as follows:

$$-\frac{1}{6}\big(\big(\phi_{[0]} - \phi_{[1]} + 4\phi_{[3]} - 4\phi_{[4]} + \phi_{[6]} - \phi_{[7]}\big)\Delta y^2 \mu\sigma + \cdots + 6\big(A_{[e0]} - 2A_{[e1]} + A_{[e7]}\big)\Delta z\big)\big/\big(\Delta y^2 \Delta z \mu\big) = 0. \quad (17)$$

Similarly, the difference form of the finite-element equation (14) for $e5$ can be written as follows:

$$-\frac{1}{6}\big(\big(\phi_{[1]} - \phi_{[2]} + 4\phi_{[4]} - 4\phi_{[5]} + \phi_{[7]} - \phi_{[8]}\big)\Delta y^2 \mu\sigma + \cdots + 6\big(A_{[e10]} - 2A_{[e5]} + A_{[e4]}\big)\Delta z\big)\big/\big(\Delta y^2 \Delta z \mu\big) = 0. \quad (18)$$

Upon taking the average of (17) and (18), one gets the averaged difference form of the finite-element equation (14) along the z-direction

$$-\frac{1}{6}\big(\big(\phi_{[0]} - \phi_{[2]} + 4\phi_{[3]} - 4\phi_{[5]} + \phi_{[6]} - \phi_{[8]}\big)\Delta y^2 \mu\sigma + \cdots + 6\big(A_{[e0]} - 2A_{[e1]} + A_{[e4]} - 2A_{[e5]} + A_{[e7]} + \cdots + A_{[e10]}\big)\Delta z\big)\big/\big(\Delta y^2 \Delta z \mu\big) = 0. \quad (19)$$

Equation (19) is in terms of the edge vectors $A_{[e]}$. By following the similar procedure that applies for (16), the edge variables are represented with their respective node equivalents:

$$-\frac{1}{6}\big(\big(\phi_{[0]} - \phi_{[2]} + 4\phi_{[3]} - 4\phi_{[5]} + \phi_{[6]} - \phi_{[8]}\big)\Delta y^2 \mu\sigma + \cdots + 12\big(A_{z[1]} - 2A_{z[4]} + A_{z[7]}\big)\Delta z\big)\big/\big(\Delta y^2 \Delta z \mu\big) = 0. \quad (20)$$

By following the same procedure for the y-directed edges, that is, the following hold: 1) obtain the difference equations of the Galerkin formulation from $e3$ and $e9$ edges; 2) average them; and 3) represent the edge variables with their node equivalents. After these three steps, the final difference equation for (13) can be written as follows:

$$-\frac{1}{6}\big(\big(\phi_{[0]} + 4\phi_{[1]} + \phi_{[2]} - \phi_{[6]} - 4\phi_{[7]} - \phi_{[8]}\big)\Delta z \mu\sigma + \cdots - 6\big(-A_{y[3]} + A_{y[5]} + A_{z[1]} - A_{z[7]}\big)\mu\sigma u_z \Delta z + \cdots + 12\big(A_{y[3]} - 2A_{y[4]} + A_{y[5]}\big)\big)\big/\big(\Delta z^2 \mu\big) + \cdots = \frac{1}{12}\big(B_{x[0]} + 4B_{x[1]} + B_{x[2]} + 2B_{x[3]} + 8B_{x[4]} + \cdots + 2B_{x[5]} + B_{x[6]} + 4B_{x[7]} + B_{x[8]}\big)\sigma u_z. \quad (21)$$

Equations (16), (20), and (21) form a system of three equations and three variables ϕ, A_y, and A_z. The stability analysis can be now performed by taking 2-D Z transform of these equations [20], [29], [31]. In this, the z-direction is represented by the transformation variable Z_n, and the y-direction is represented by the transformation variable Z_m [please refer to Fig. 4(b)]. After taking 2-D Z transform, (16), (21), and (20) take the following form:

$$\frac{1}{3}[S1]\phi + \frac{u_z}{4}[S2]A_y - \frac{u_z}{2}[S3]A_z = \frac{u_z \Delta z}{12}[Q1]B_x \quad (22)$$

$$\frac{Pe}{6u_z}[Q1]\phi + (-[S1] + Pe[Q2])A_y + Pe[S3]A_z + \cdots = \frac{Pe\,\Delta z}{12}[M1]B_x \quad (23)$$

$$\frac{Pe}{6u_z}\big[Q2'\big]\phi - \big[S1'\big]A_z = 0 \quad (24)$$

where

$$[Q1] = Z_n^2 Z_m^2 + 4Z_n Z_m^2 + Z_m^2 - Z_n^2 - 4Z_n - 1 \quad (25)$$
$$[Q2] = Z_n^2 Z_m - Z_m \quad (26)$$
$$[Q2'] = Z_n^2 Z_m^2 - Z_m^2 + 4Z_n^2 Z_m - 4Z_m + Z_n^2 - 1 \quad (27)$$
$$[S1] = 1 + Z_n + Z_n^2 + Z_m + Z_n^2 Z_m + Z_m^2 + \cdots + Z_n Z_m^2 + Z_n^2 Z_m^2 - 8Z_n Z_m \quad (28)$$
$$[S2] = 1 + Z_n^2 Z_m^2 - Z_n^2 - Z_m^2 \quad (29)$$
$$[S3] = Z_n - Z_n Z_m^2 \quad (30)$$
$$[S1'] = Z_n - 2Z_n Z_m + Z_n Z_m^2 \quad (31)$$
$$[M1] = 1 + 4Z_n + Z_n^2 + 2Z_m + 8Z_n Z_m + \cdots + 2Z_n^2 Z_m + Z_m^2 + 4Z_n Z_m^2 + Z_n^2 Z_m^2. \quad (32)$$

Equations (22), (23), and (24) form a system of three equations with three variables ϕ, A_y, and A_z. By following a similar procedure as that of [20], the final equation is obtained for $Pe \gg 1$ as follows:

$$\left([Q2][S3] + \frac{[S3][S2]}{2}\right) A_y \approx \frac{\Delta z}{12}([M1][S3] + \cdots + 2[Q1][S3]) B_x. \quad (33)$$

Upon simplification, the transfer function takes the following form:

$$\frac{A_y}{B_x} \approx \frac{\Delta z}{6} \frac{\left(Z_n^2 + 4Z_n + 1\right) f1(Z_m)}{\left(1 - Z_n^2\right) f2(Z_m)} \quad (34)$$

where

$$f1(Z_m) = 1 - 2Z_m - 3Z_m^2$$
$$f2(Z_m) = \left(2Z_m - \left(1 - Z_m^2\right)^2\right).$$

The transfer function (34) has *poles/roots* located at -1 and $+1$, among which the pole at "-1" causes the oscillatory behavior in the solution. The *zeros* are located at $Z_n = -0.27$ and -3.7. The locations of the zeros may be changed by modifying the representation of the input magnetic field consistently. By following the 1-D case (please refer to Section II-A) and the preceding work [20], the input magnetic field, which is directed along x edges (perpendicular to the plane), can be averaged over each element, and the resultant magnetic field can be used as the input field. In other words, the following would be the input field for the element $E1$:

$$B_x = \frac{1}{4}(B_x[n-1, m-1] + B_x[n, m-1] + \cdots + B_x[n-1, m] + B_x[n, m]) \quad (35)$$

and similarly for other elements. With this modification, the transfer function for the proposed formulation is calculated to take the following form:

$$\frac{A_y}{B_x} \approx \frac{\Delta z}{4} \frac{\left(Z_n^2 + 2Z_n + 1\right) f1(Z_m)}{\left(1 - Z_n^2\right) f2(Z_m)} \approx \frac{\Delta z}{4} \frac{(1 + Z_n)\cancel{(1 + Z_n)} f1(Z_m)}{(1 - Z_n)\cancel{(1 + Zn)} f2(Z_m)}. \quad (36)$$

The oscillatory pole at "$Z = -1$" is canceled by the zero introduced in the numerator. Thus, the elemental averaging of the input magnetic field can be seen to possess the stability properties similar to that of 1-D. In Section III, numerical validation exercises are carried out in 2-D and 3-D.

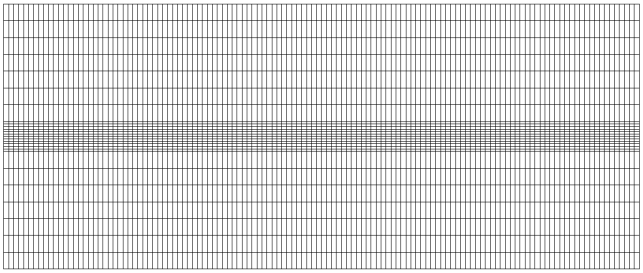

Fig. 5. Sample 2-D finite-element mesh.

III. Numerical Validation

A. Simulation Results for 2-D Version of the Problem

The 2-D simulation involves the problem setup, shown in Fig. 1. The corresponding finite-element mesh is shown in Fig. 5. The physical parameters of the problem are as follows. The conductor has a width of $d = 0.5$ m, its conductivity is $\sigma = 7.2 \times 10^6$ Sm^{-1}, and its velocity is $u_z = 50$ ms^{-1}. Simulations were carried out to test the stability of the proposed formulation; stable solutions are observed. A sample simulation result showing the reaction magnetic field $b_x = \partial A_z/\partial y - \partial A_y/\partial z$ with $Pe = 200$ is displayed in Fig. 6. Fig. 6(a) shows the b_x obtained from the standard Galerkin formulation, and Fig. 6(b) shows the same from the proposed formulation. It can be seen that the proposed formulation gives a stable solution without any numerical oscillations.

In the nodal formulation, it was possible to obtain the analytical expression for the peak errors due to the numerical oscillation [20]. This is because, the nodal formulation can be reduced to 1-D, and the resulting finite-element equation in the difference form can be solved. The following expressions of peak errors are derived in [20].

Analytical error in the standard Galerkin formulation

$$\hat{e}_{\mathrm{GA}} = \left| \frac{\left(Pe^2 - 3\right)(Pe - 1)}{3(Pe + 1)^3} \right| \times 100\%. \quad (37)$$

Analytical error in the stable nodal formulation of [20]

$$\hat{e}_{\mathrm{SA}} = \left| \frac{Pe - 1}{(Pe + 1)^3} \right| \times 100\%. \quad (38)$$

Having these nodal errors as a reference, the peak oscillation error with the edge elements is measured for the 2-D problem. These measured values are plotted in Fig. 7, where $\hat{e}_{\mathrm{GN}}$ is the peak error measured with the Galerkin formulation and $\hat{e}_{\mathrm{SN}}$ is the peak error measured with the proposed formulation. It is observed that the peak error from the 2-D Galerkin edge is twice that of the 1-D Galerkin node. In other words, "$\hat{e}_{\mathrm{GN}} \approx 2\hat{e}_{\mathrm{GA}}$" and the same can be observed from the plot of "$2\hat{e}_{\mathrm{GA}}$" in Fig. 7. It can also be observed that the peak error measured with the proposed formulation ($\hat{e}_{\mathrm{SN}}$) is negligible.

In Table I, the average and the rms error measured for the first derivative (reaction magnetic field b_x) are presented.

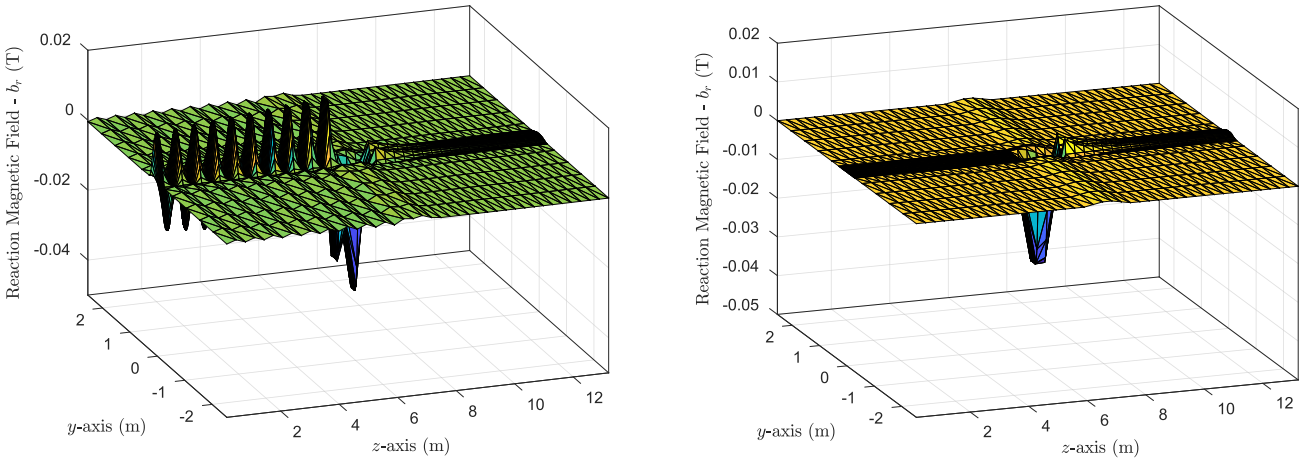

Fig. 6. Reaction magnetic field—b_x from the 2-D moving conductor problem with $Pe = 200$. (a) Galerkin formulation. (b) Proposed formulation.

TABLE I
MEASURED VALUES OF ERROR IN THE FIRST DERIVATIVE FOR THE GALERKIN SCHEME AND THE PROPOSED SCHEME

Number of Elements	Pe	Error measured in $b_x = \nabla \times \mathbf{A} \cdot \hat{x}$, normalised w.r.t. applied magnetic field B_{ax}					
		Galerkin Formulation			Proposed Formulation		
		L2 Error	Absolute Error	Expt. Order of Convergence	L2 Error	Absolute Error	Expt. Order of Convergence
640	100	6.035e-04	1.213e-01	-	1.765e-04	1.594e-02	-
2560	50	4.634e-04	8.741e-02	0.47	1.210e-04	8.650e-03	0.88
10240	25	2.708e-04	4.327e-02	1.01	7.919e-05	3.988e-03	1.12
40960	12.5	1.218e-04	1.220e-02	1.83	4.558e-05	1.509e-03	1.40

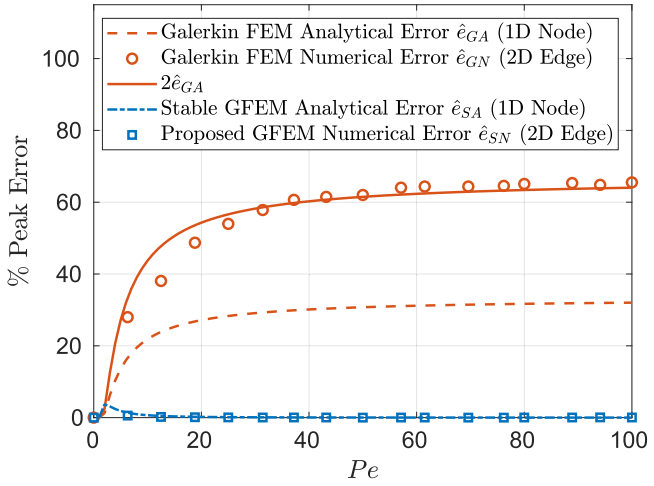

Fig. 7. Percentage of peak error measured.

The errors are measured for the Galerkin scheme and the proposed scheme, for different amounts of resolution. The average error and the rms ($L2$) error are observed to fall with the increasing resolution. It may also be noted that the errors measured from the proposed scheme are an order of magnitude smaller than the errors measured from the Galerkin scheme. With the increasing resolution, the proposed formulation also produces the expected convergence rate. Thus, the proposed formulation gives stable as well as accurate results.

In Section III-B, further testing is carried out in 3-D with the "Testing Electromagnetic Analysis Methods" (TEAMs) problem No. 9 [32].

B. Validation With 3-D TEAM-9 Problem

A schematic of the TEAM-9 problem is shown in Fig. 8(a). The problem has an infinite ferromagnetic material with the conductivity of $\sigma = 5 \times 10^6$ Sm^{-1}. The relative magnetic permeability of the material is taken as $\mu_r = 1$ and $\mu_r = 50$. The ferromagnetic material has a cylindrical bore with the radius of $r_i = 14 \times 10^{-3}$ m. A concentric current-carrying loop with 1 A of current and a radius of $r_c = 12 \times 10^{-3}$ m is moving at an uniform velocity inside the bore. For the analysis, the case with the largest velocity ($v = 100$ ms^{-1}) is chosen. In order to accurately model the current loop, the finite-element mesh close to the current loop is dense; away from the current loop, the mesh becomes progressively coarser. Due to this variation, the resulting value of the Peclet number varies from 5 to 200. The finite-element mesh employed is shown in Fig. 8(b).

In the proposed formulation, for each element, the x, y, z components of the applied magnetic field B_x, B_y, and B_z are represented as follows:

$$B_x = \frac{1}{\sum_{e=1}^{n} \left| v_x^e \right|} \sum_{e=1}^{n} B^e v_x^e \tag{39}$$

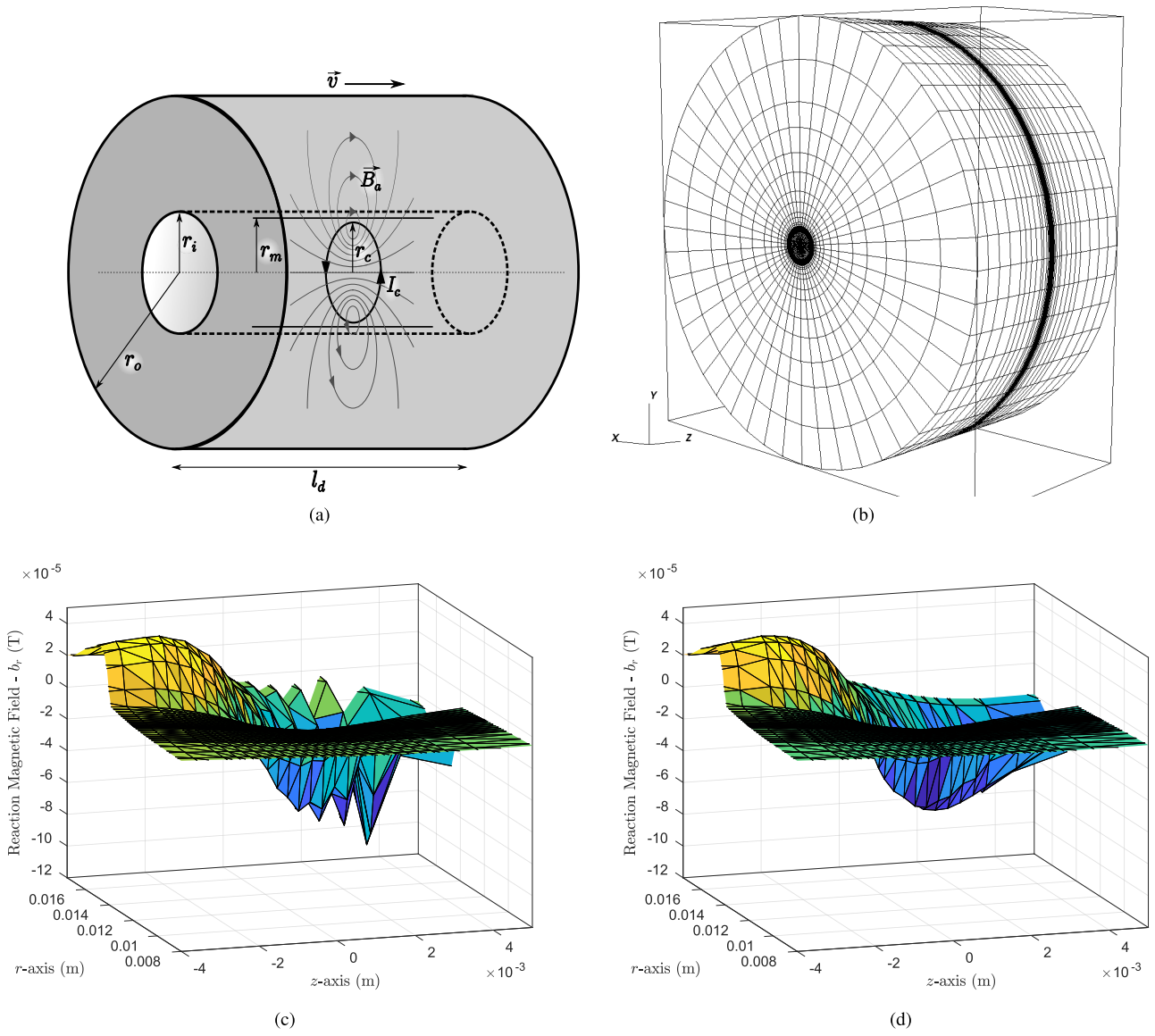

Fig. 8. Description of the TEAM 9a problem and sample results. (a) Schematic representation of the TEAM 9a moving conductor problem. (b) Finite-element mesh employed. (c) Galerkin scheme—reaction magnetic field—b_r for $u_z = 100$ ms^{-1} and $\mu_r = 50$. (d) Proposed scheme—reaction magnetic field—b_r for $u_z = 100$ ms^{-1} and $\mu_r = 50$ in the cross section along the rz plane for $\theta \approx 0°$.

$$B_y = \frac{1}{\sum_{e=1}^{n} |v_y^e|} \sum_{e=1}^{n} B^e v_y^e \tag{40}$$

$$B_z = \frac{1}{\sum_{e=1}^{n} |v_z^e|} \sum_{e=1}^{n} B^e v_z^e \tag{41}$$

where n is the number of edges for each element; B^e is the applied magnetic field corresponding to each edge; and v_x^e, v_y^e, and v_z^e form the unit vector $\mathbf{v}_e = \{v_x^e, v_y^e, v_z^e\}$ of the edge "e." The elemental applied magnetic field vector $\mathbf{B} = \{B_x, B_y, B_z\}$ is the source field in the proposed formulation.

The standard Galerkin formulation would have the applied magnetic field at each Gauss-integration point $\mathbf{B}_g$ as follows:

$$\mathbf{B}_g = \sum_{e=1}^{n} B^e \mathbf{M}_g^e$$

where $\mathbf{M}_g^e$ is the value of edge shape function vector at a Gauss-integration point. The simulated, reaction magnetic field along the rz plane is plotted in Fig. 8(c) and (d) for the Galerkin scheme and the proposed formulation, respectively. It may be readily noted that the b_r from the proposed formulation is stable as expected.

The TEAM-9 test problem is also provided with the set of analytical solution for comparison [32]. It may be noted that, the analytical solutions are provided along the radius of $r = 13$ mm, which is 1 mm away from both the current-carrying coil and the ferromagnetic cylinder. Since the measurement point is very close to the cylinder as well as the circular coil, it is necessary to model them as accurately as possible. Such a modeling is not feasible with linear edge elements in a cartesian coordinate system. Therefore, the problem is transferred to the cylindrical coordinate system for the accuracy study. In the cylindrical coordinate system, the results of Fig. 8(c) and (d) are once again observed. In addition to this, edge elements can accurately represent the simulation

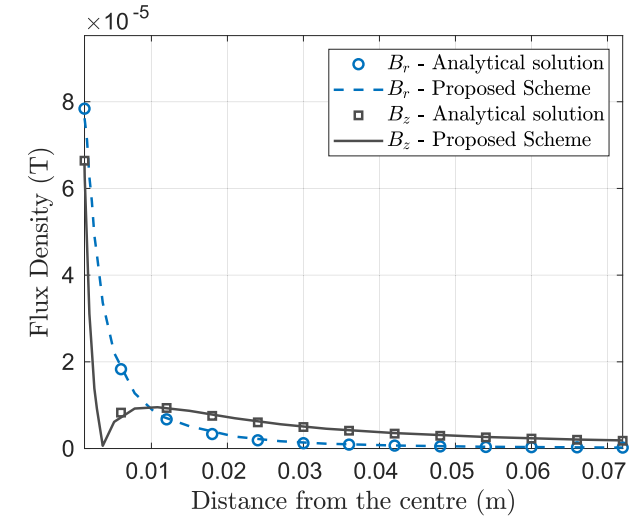

(a)

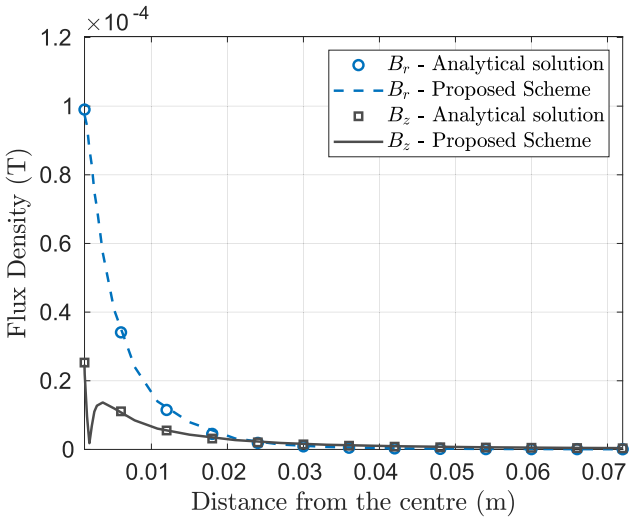

(b)

Fig. 9. Comparison of the total magnetic flux densities from the analytical solution of the TEAM-9 problem [32] and the proposed formulation, for the cases of (a) $u_z = 100$ ms^{-1}, $\mu_r = 1$ and (b) $u_z = 100$ ms^{-1}, $\mu_r = 50$.

domain in the cylindrical coordinate system. Simulations are carried out for $v = 100$ ms^{-1} with $\mu_r = 1$ as well as the ferromagnetic case of $\mu_r = 50$. The results from $r = 13$ mm are plotted along with the analytical solution in Fig. 9. It can be seen that the proposed formulation performs consistently in 3-D as well.

IV. Discussion on Mesh

This work deals with the simulation of linear moving conductor problems, such as electromagnetic brakes, linear induction motor, electromagnetic flowmeter, and so on. In such cases, the conducting region of the problem can be and usually be discretized with graded regular mesh along the moving direction. In other words, the resulting mesh would look like a stack of layers of different thickness along the moving direction. The same can be seen in Fig. 8(b). In this, the discretization along the direction of motion (z-axis) has dense discretization close to the center, where the current loop is present and the discretization becomes coarser as we move away from the center.

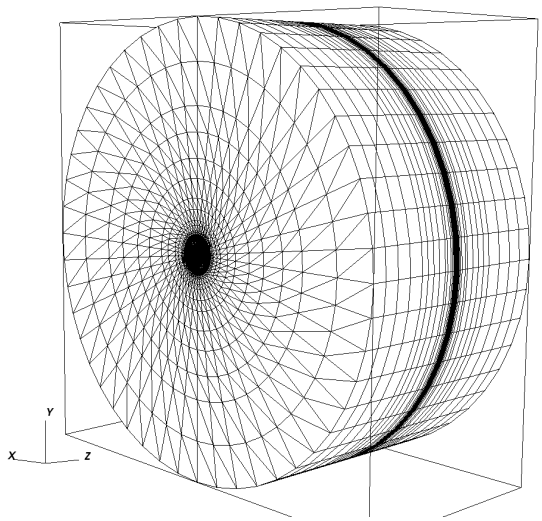

(a)

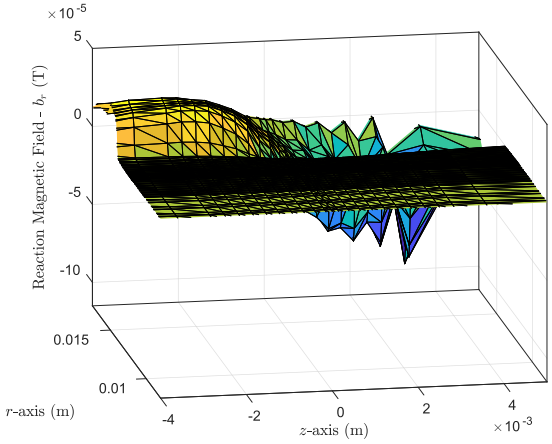

(b)

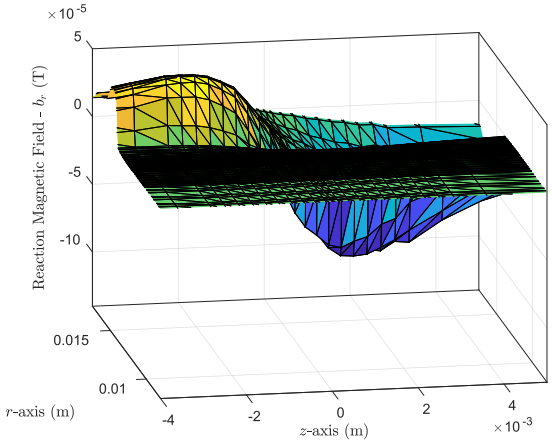

(c)

Fig. 10. Sample results from TEAM 9a problem with wedge elements. (a) Finite-element mesh with wedge elements. (b) Galerkin scheme—reaction magnetic field—b_r for $u_z = 100$ ms^{-1} and $\mu_r = 50$. (c) Proposed scheme—reaction magnetic field—b_r for $u_z = 100$ ms^{-1} and $\mu_r = 50$ in the cross section along the rz plane for $\theta \approx 0°$.

The source-based stabilization strategies utilize this feature of the linear moving conductor problems. Here, the stabilization is brought in by the pole-zero cancellation of the source term. Such an analysis is valid, only when the discretization is like a stack of layers along the moving direction. Hence, the proposed scheme requires a regular mesh in 2-D with quadrilateral elements. In the case of 3-D, the restriction only applies to the direction of motion. Therefore, the cross section of the moving conductor, i.e., the plane perpendicular to the motion, can be discretized without any restrictions. Hence, the 3-D problems can be discretized with hexahedral or wedge elements. The discretization using hexahedral elements is shown in Fig. 8(b).

The application of wedge elements with vector shape functions is scarce in literature. However, the vector shape functions for the wedge elements are straightforward to derive, and they are provided in the Appendix for reference. The discretization using wedge elements for the TEAM-9 test problem is shown in Fig. 10(a). The simulated reaction magnetic field, along the rz plane, is plotted in Fig. 10(b) and (c) for the Galerkin scheme and the proposed formulation, respectively. The b_r from the proposed formulation is stable as expected, with the wedge elements as well. As an added note, the discussion in this section is also applicable to node elements [20].

V. Conclusion

Edge elements are vital in the finite-element simulation of electromagnetic fields, especially when multiple materials are present and the simulation variables are electric and magnetic fields themselves. Similar to many other central-weighted numerical schemes, edge elements also produce numerically oscillating solutions for the simulation of moving conductor problems at high velocities. In such a situation, the usual strategy is to employ the upwinding strategies, which in a way introduce extra diffusion to stabilize the solution [18], [22], [23]. However, the upwinding schemes are known to be susceptible to transverse-boundary error at the material interfaces [21], [24], [25], [27].

In this work, the source-based stabilization strategies, which are proposed for the nodal formulation, are extended for the edge elements. The formulation requires a graded regular mesh along the direction of motion. The stability of the proposed formulation is analytically studied in 1-D as well as 2-D with edge elements. Then, numerical exercises are carried out for the verification of the proposed formulation. The simulation results in 2-D demonstrate that the formulation produces stable, accurate, and converging solutions. The 3-D simulation is carried out with the TEAM-9 problem, and stable solutions are observed. Comparing the analytical solutions of the TEAM-9 problem and the simulation results, accuracy of the proposed formulation is demonstrated in 3-D.

Appendix
Wedge Element—Vector Shape Functions

The edge shape functions for the wedge element are provided below. Consider the reference triangle element in the (ξ, η) coordinate system with its nodes a, b, c located at $(0, 0)$, $(1, 0)$, and $(0, 1)$, respectively. The node shape functions for this reference triangle element can be written as follows [33]:

$$\begin{aligned} N_a &= 1 - \xi - \eta \\ N_b &= \xi \\ N_c &= \eta. \end{aligned} \tag{42}$$

Using these, the vector shape function of the wedge element can be constructed. The reference wedge element in the (ξ, η, ζ) coordinate system is shown in Fig. 11. The edge shape functions for the wedge element are

$$\begin{aligned} \mathbf{M_1} &= l_1(N_a\nabla N_b - N_b\nabla N_a)\frac{(1-\zeta)}{2} \\ \mathbf{M_2} &= l_2(N_b\nabla N_c - N_c\nabla N_b)\frac{(1-\zeta)}{2} \\ \mathbf{M_3} &= l_3(N_c\nabla N_a - N_a\nabla N_c)\frac{(1-\zeta)}{2} \\ \mathbf{M_4} &= l_4(N_a\nabla N_b - N_b\nabla N_a)\frac{(1+\zeta)}{2} \\ \mathbf{M_5} &= l_5(N_b\nabla N_c - N_c\nabla N_b)\frac{(1+\zeta)}{2} \\ \mathbf{M_6} &= l_6(N_c\nabla N_a - N_a\nabla N_c)\frac{(1+\zeta)}{2} \\ \mathbf{M_7} &= l_7 N_a\nabla\zeta/2 \\ \mathbf{M_8} &= l_8 N_b\nabla\zeta/2 \\ \mathbf{M_9} &= l_9 N_c\nabla\zeta/2 \end{aligned} \tag{43}$$

where $l_1, l_2, \ldots, l_9$ are the actual lengths of the edges that correspond to edge shape function $\mathbf{M}$. The gradients are taken with respect to the (x, y, z) coordinate system [28].

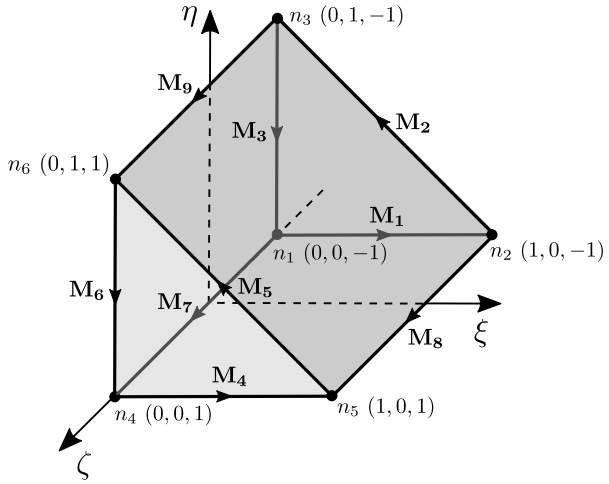

Fig. 11. Wedge element in the (ξ, η, ζ) coordinate system. n denotes the nodes of the element. $\mathbf{M}$ denotes the vector shape functions and corresponds to each edge.

References

[1] O. Biro, K. Preis, W. Renhart, K. R. Richter, and G. Vrisk, "Performance of different vector potential formulations in solving multiply connected 3-D eddy current problems," *IEEE Trans. Magn.*, vol. 26, no. 2, pp. 438–441, Mar. 1990.

[2] T. Shimizu, N. Takeshima, and N. Jimbo, "A numerical study on Faraday-type Electromagnetic Flowmeter in liquid metal system, (I)," *J. Nucl. Sci. Technol.*, vol. 37, no. 12, pp. 1038–1048, Dec. 2000.

[3] O. Zienkiewicz, R. Taylor, and P. Nithiarasu, *The Finite Element Method for Fluid Dynamics*. Amsterdam, The Netherlands: Elsevier, 2005.
[4] D. B. Spalding, "A novel finite difference formulation for differential expressions involving both first and second derivatives," *Int. J. Numer. Methods Eng.*, vol. 4, no. 4, pp. 551–559, Jul. 1972.
[5] I. Christie, D. F. Griffiths, A. R. Mitchell, and O. C. Zienkiewicz, "Finite element methods for second order differential equations with significant first derivatives," *Int. J. Numer. Methods Eng.*, vol. 10, no. 6, pp. 1389–1396, 1976.
[6] M. Odamura, "Upwind finite element solution for saturated traveling magnetic field problems," *Electr. Eng. Jpn.*, vol. 105, no. 4, pp. 126–132, 1985.
[7] M. Ito, T. Takahashi, and M. Odamura, "Up-wind finite element solution of travelling magnetic field problems," *IEEE Trans. Magn.*, vol. 28, no. 2, pp. 1605–1610, Mar. 1992.
[8] D. Rodger, P. J. Leonard, and T. Karaguler, "An optimal formulation for 3D moving conductor eddy current problems with smooth rotors," *IEEE Trans. Magn.*, vol. 26, no. 5, pp. 2359–2363, Sep. 1990.
[9] E. K. C. Chan and S. Williamson, "Factors influencing the need for upwinding in two-dimensional field calculation," *IEEE Trans. Magn.*, vol. 28, no. 2, pp. 1611–1614, Mar. 1992.
[10] N. Allen, D. Rodger, P. C. Coles, S. Strret, and P. J. Leonard, "Towards increased speed computations in 3D moving eddy current finite element modelling," *IEEE Trans. Magn.*, vol. 31, no. 6, pp. 3524–3526, Nov. 1995.
[11] D. Rodger, T. Karguler, and P. J. Leonard, "A formulation for 3D moving conductor eddy current problems," *IEEE Trans. Magn.*, vol. 25, no. 5, pp. 4147–4149, Sep. 1989.
[12] J. Bird and T. A. Lipo, "A 3-D magnetic charge finite-element model of an electrodynamic wheel," *IEEE Trans. Magn.*, vol. 44, no. 2, pp. 253–265, Feb. 2008.
[13] H. V. Sande, H. De Gersem, and K. Hameyer, "Finite element stabilization techniques for convection-diffusion problems," *Int. J. Theor. Electrotechnics*, pp. 56–59, Mar. 1999.
[14] L. Codecasa and P. Alotto, "2-D stabilized FIT formulation for eddy-current problems in moving conductors," *IEEE Trans. Magn.*, vol. 51, no. 3, pp. 1–4, Mar. 2015.
[15] Y. Liang, "Steady-state thermal analysis of power cable systems in ducts using streamline-upwind/Petrov–Galerkin finite element method," *IEEE Trans. Dielectr. Electr. Insul.*, vol. 19, no. 1, pp. 283–290, Feb. 2012.
[16] S. Noguchi and S. Kim, "Magnetic field and fluid flow computation of plural kinds of magnetic particles for magnetic separation," *IEEE Trans. Magn.*, vol. 48, no. 2, pp. 523–526, Feb. 2012.
[17] T.-P. Fries and H. G. Matthies, "A review of Petrov–Galerkin stabilization approaches and an extension to meshfree methods," Techn. Univ. Braunschweig, Brunswick, Germany, Tech. Rep. 2004-01, 2004.
[18] E. Oñate and M. Manzan, "Stabilization techniques for finite element analysis of convection-diffusion problems," *Develop. Heat Transf.*, vol. 7, pp. 71–118, Feb. 2000.
[19] S. Subramanian and U. Kumar, "Augmenting numerical stability of the Galerkin finite element formulation for electromagnetic flowmeter analysis," *IET Sci., Meas. Technol.*, vol. 10, no. 4, pp. 288–295, Jul. 2016.
[20] S. Subramanian and U. Kumar, "Stable Galerkin finite-element scheme for the simulation of problems involving conductors moving rectilinearly in magnetic fields," *IET Sci., Meas. Technol.*, vol. 10, no. 8, pp. 952–962, 2016.
[21] S. Subramanian, U. Kumar, and S. Bhowmick, "On overcoming the transverse boundary error of the SU/PG scheme for moving conductor problems," *IEEE Trans. Magn.*, vol. 58, no. 1, pp. 1–8, Jan. 2022.
[22] E. X. Xu, J. Simkin, and S. C. Taylor, "Streamline upwinding in a 3-D edge-element method modeling eddy currents in moving conductors," *IEEE Trans. Magn.*, vol. 42, no. 4, pp. 667–670, Apr. 2006.
[23] F. Henrotte, H. Heumann, E. Lange, and K. Hameyer, "Upwind 3-D vector potential formulation for electromagnetic braking simulations," *IEEE Trans. Magn.*, vol. 46, no. 8, pp. 2835–2838, Aug. 2010.
[24] S. Subramanian and S. Bhowmick, "A stable weighted residual finite element formulation for the simulation of linear moving conductor problems," *IEEE J. Multiscale Multiphys. Comput. Techn.*, vol. 7, pp. 220–227, 2022.
[25] V. John and P. Knobloch, "On spurious oscillations at layers diminishing (SOLD) methods for convection–diffusion equations: Part I—A review," *Comput. Methods Appl. Mech. Eng.*, vol. 196, nos. 17–20, pp. 2197–2215, Mar. 2007.
[26] V. John and P. Knobloch, "On spurious oscillations at layers diminishing (SOLD) methods for convection–diffusion equations: Part II—Analysis for $P1$ and $Q1$ finite elements," *Comput. Methods Appl. Mech. Eng.*, vol. 197, no. 21, pp. 1997–2014, 2008.
[27] S. Subramanian and U. Kumar, "Existence of boundary error transverse to the velocity in SU/PG solution of moving conductor problem," in *IEEE MTT-S Int. Microw. Symp. Dig.*, Jul. 2016, pp. 1–2.
[28] J.-M. Jin, *The Finite Element Method in Electromagnetics*. Hoboken, NJ, USA: Wiley, 2002.
[29] A. D. Poularikas, *Handbook Formulas Tables for Signal Process*, vol. 13. Boca Raton, FL, USA: CRC Press, 1998.
[30] D. Dudgeon and R. M. Mersereau, *Multidimensional Digital Signal Processing*. Upper Saddle River, NJ, USA: Prentice-Hall, 1995.
[31] K. Ogata, *Discrete-Time Control Systems*. Upper Saddle River, NJ, USA: Prentice-Hall, 1987.
[32] N. Ida, "Team problem 9 velocity effects and low level fields in axisymmetric geometries," in *Proc. Vancouver TEAM Workshop*, Jul. 1988, pp. 1–19.
[33] J. Reddy, *An Introduction to the Finite Element Method*. New York, NY, USA: McGraw-Hill, 2005.

Sujata Bhowmick (Member, IEEE) received the B.E. degree in electrical engineering from the Indian Institute of Engineering Science and Technology Shibpur, Howrah, India, in 2006, the M.E. degree in electrical engineering from the Indian Institute of Science, Bengaluru, India, in 2011, and the Ph.D. degree from the Department of Electronic Systems Engineering, Indian Institute of Science, in 2019.

Her current research interests include power electronics for renewable resources, single-phase grid-connected power converters, computational electromagnetics, and finite-element and edge-element methods.

Sethupathy Subramanian received the bachelor's degree in electrical and electronics engineering from Anna University, Chennai, India, in 2009, the master's and Ph.D. degrees in electrical engineering from the Indian Institute of Science, Bangaluru, India, in 2011 and 2017, respectively, and the master's and Ph.D. degrees in physics from the University of Notre Dame, Notre Dame, IN, USA, in 2022 and 2023, respectively.

His research interests, pertinent to electrical engineering, include computational electromagnetics, numerical stability, and finite-element and edge-element methods.